

Article

# Promoting Effect of Ti Species in MnO<sub>x</sub>-FeO<sub>x</sub>/Silicalite-1 for the Low-Temperature NH<sub>3</sub>-SCR Reaction

Jialiang Gu <sup>1</sup>, Rudi Duan <sup>1</sup>, Weibin Chen <sup>1</sup>, Yan Chen <sup>2</sup>, Lili Liu <sup>1</sup> and Xidong Wang <sup>1,\*</sup>

<sup>1</sup> Beijing Key Laboratory for Solid Waste Utilization and Management, Department of Energy and Resources Engineering, College of Engineering, Peking University, Beijing 100871, China; jialiang\_gu@pku.edu.cn (J.G.); duanrudi912@163.com (R.D.); chenwb@pku.edu.cn (W.C.); liu-0806@163.com (L.L.)

<sup>2</sup> State Key Joint Laboratory of Environment Simulation and Pollution Control, School of Environment, Tsinghua University, Beijing 100084, China; ychen1990@126.com

\* Correspondence: xidong@pku.edu.cn; Tel.: +86-10-8252-9083

Received: 28 April 2020; Accepted: 13 May 2020; Published: 19 May 2020



**Abstract:** Manganese and iron oxides catalysts supported on silicalite-1 and titanium silicalite-1 (TS-1) are synthesized by the wet impregnation method for the selective catalytic reduction (SCR) of NO<sub>x</sub> with NH<sub>3</sub> (NH<sub>3</sub>-SCR), respectively. The optimized catalyst demonstrates an increased NO<sub>x</sub> conversion efficiency of 20% below 150 °C, with a space velocity of 18,000 h<sup>-1</sup>, which can be attributed to the incorporation of Ti species. The presence of Ti species enhances surface acidity and redox ability of the catalyst without changing the structure of supporter. Moreover, further researches based on in situ NH<sub>3</sub> adsorption reveal that Lewis acid sites linked to Mn<sup>4+</sup> on the surface have a huge influence on the improvement of denitration efficiency of the catalyst at low temperatures.

**Keywords:** denitration; silicalite-1; titanium; NH<sub>3</sub>-SCR

## 1. Introduction

Nitrogen oxides (NO<sub>x</sub>) bring out a series of environmental problems, such as photochemical pollution, acid rain and haze, which seriously threaten human health [1,2]. Nowadays, selective catalytic reduction (SCR) with NH<sub>3</sub> has been proved to be an effective technology for NO<sub>x</sub> emission control, which has been widely used in coal-fired power plants [3–5]. Commercial V<sub>2</sub>O<sub>5</sub>-WO<sub>3</sub>/TiO<sub>2</sub> catalysts are very suitable for power plants, mainly due to the flue gas there, with a high temperature (>300 °C), which can satisfy the required reaction temperature of the catalyst. However, there are still a large number of untreated NO<sub>x</sub> derived from industrial activities such as cement kilns, steel sintering and waste incinerators, where the temperature of flue gas is too low (<200 °C) to suit for these commercial catalysts [6,7]. Therefore, it is urgent to develop novel high-efficient catalysts, which have high catalytic activities at low temperatures.

Manganese-based catalysts are proved to be excellent denitration catalysts at low temperatures among the commonly used transition metal oxide catalysts [8–10]. Furthermore, numerous metals, like Fe, Ce and Cu, are used as active components to modify manganese-based catalysts, and for that purpose, the single manganese oxides can only maintain high denitrification activities in a narrow temperature window, accompanied by several side reactions [11–14]. In addition, proper supporters can not only provide a huge surface to disperse the active components, but can also supply abundant adsorption sites for the heterogeneous reactions [15,16]. Both Al<sub>2</sub>O<sub>3</sub> and TiO<sub>2</sub> have been widely investigated as common supporters in the last few decades. However, the limited specific surface area, as well as poor water and sulfur resistance of the catalysts, hinder their further developments in industrial applications [17,18]. At the same time, carbon-based materials are also

applied as supporters of catalysts, because of their large surface area, unique porous structure and abundant oxygen functional groups. Nevertheless, the poor thermal stability and oxidizability of carbon-based materials are a potential safety hazard in industrial applications [19–21]. In recent years, zeolites have gained widespread attention as supporters in SCR studies, due to their high thermal stability, unique porous structure and absence of harmful substances [22–24]. Wang et al. [25] found that the optimized Mn-Fe/ZSM achieved 100% NO<sub>x</sub> conversion efficiencies from 150 °C to 250 °C. The excellent catalytic performance can be attributed to the addition of iron, which increases the levels of Mn<sup>4+</sup> and oxygen vacancy. Nevertheless, the presence of Al species in ZSM-5 makes contributions to its strong hydrophilicity, which hinders its applications in industrial denitration, because the flue gas is usually humid. However, silicalite-1 is reported to exhibit excellent water resistance in an NH<sub>3</sub>-SCR reaction, which can be attributed to the decrease in hydrophilicity due to the absence of heteroatoms [26,27]. However, compared with ZSM-5, the surface acidity of silicalite-1 is a little bit weaker, which is the key to the low-temperature denitration. To date, Ti atoms have been reported to replace a small amount of Si atoms for improving the surface acidity and maintaining excellent water resistance, which can benefit the low-temperature denitration [28].

Herein, we introduce novel high-efficient denitration catalysts with highly dispersed MnO<sub>x</sub> and FeO<sub>x</sub> nanoparticles supported on silicalite-1 and titanium silicalite-1 (TS-1) respectively. Compared to the catalyst supported on silicalite-1, the catalyst supported on TS-1 demonstrates superior NO<sub>x</sub> conversion efficiencies in the NH<sub>3</sub>-SCR reaction at low temperatures, which can be attributed to the incorporation of Ti species, without changing the structure of zeolites. Moreover, further researches on the surface properties of catalysts including their acidity, redox ability and in-situ adsorption, reveal that the presence of Ti species promotes the formation of Mn<sup>4+</sup> on the surface, thereby increasing the acidity and redox ability of the catalyst, which are beneficial for the low-temperature denitration.

## 2. Results and Discussion

### 2.1. Chemical Compositions and Textural Properties of Samples

The chemical compositions of the catalysts are summarized in Table 1, based on the results of ICP-OES. The mass ratios of active metal oxides are close to the initial feed ratios. The contents of Mn and Fe species make no significant difference among all the catalysts.

**Table 1.** Chemical compositions of samples.

Sample	The Mass Fraction of Metal Elements/wt.%		
	Mn	Fe	Ti
Mn <sub>3</sub> Fe <sub>2</sub> /Silicalite-1	3.18	1.87	-
Mn <sub>3</sub> Fe <sub>2</sub> /TS-1-30	3.17	1.97	2.23
Mn <sub>3</sub> Fe <sub>2</sub> /TS-1-20	3.11	1.94	3.56

The X-ray diffraction (XRD) patterns of the supporters are shown in Figure 1a. All of the supporters display obvious characteristic peaks at 7.9°, 8.8°, 23.1°, 23.8° and 24.3°, which can be attributed to a typical Mobil Five Instructure (MFI) structure. The pattern of anatase at 25.4° does not appear in TS-1-30, while it is found in TS-1-20, which indicates that the excessive Ti species form a small amount of anatase in TS-1-20. The existing form of Ti species in the supporters is further confirmed by Fourier transform infrared (FT-IR). As shown in Figure 2, the bands at 433, 545–546, 799–803, 1074–1075 and 1223–1225 cm<sup>-1</sup> can be assigned to the characteristic peaks of MFI structure; the bands at 957–958 cm<sup>-1</sup> can be the evidence for the incorporation of Ti species into frameworks [29]. Moreover, it can be seen from Figure 1b that there is no peak relevant to metal oxides in the supported catalysts, due to the extremely low metal loading of the catalysts. However, all the supported catalysts possess clear peaks that are consistent with corresponded supporters, which reveals that the supported catalysts remain the same structure with the supporters after the impregnation process [25,30].

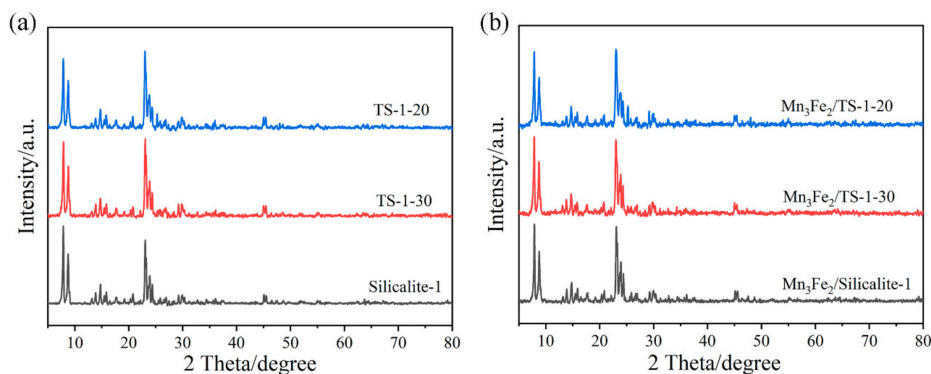


**Figure 1.** X-ray diffraction (XRD) patterns of supports (a) and catalysts (b).

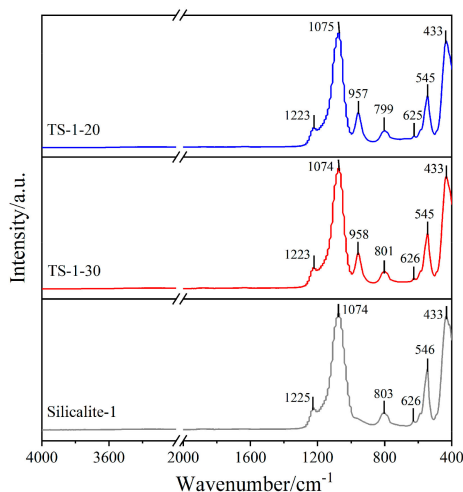


**Figure 2.** Fourier transform infrared (FT-IR) spectra of supports.

N<sub>2</sub> adsorption/desorption isotherms of the samples are illustrated in Figure 3, and the corresponding textural properties of the samples are summarized in Table 2. The isotherms can be classified as type I, indicating that all the samples have microporous structures [31,32]. The specific surface area, total pore volume and average pore diameter of Silicalite-1 are 454.31 m<sup>2</sup>/g, 0.32 cm<sup>3</sup>/g and 2.85 nm, respectively. When Ti species are introduced into the structure of zeolites, both TS-1-30 and TS-1-20 show an increase of 10% in specific surface area, total pore volume and average pore diameter, which can be attributed to the difference of atom size between Ti and Si [29]. After loading MnO<sub>x</sub> and FeO<sub>x</sub>, both specific surface area and total pore volume have a decrease of 10%, while average pore diameter remains constant, indicating that most of MnO<sub>x</sub> and FeO<sub>x</sub> species coexist on the surface, without changing the textural properties of supports, as proposed in XRD analysis [30].

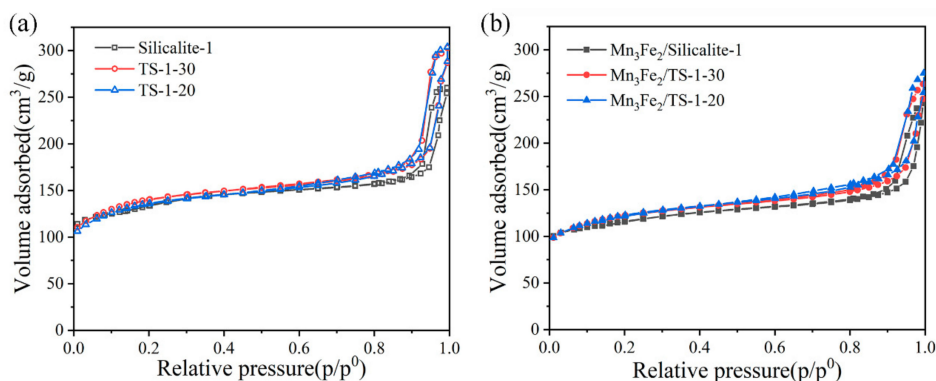


**Figure 3.** N<sub>2</sub> adsorption/desorption isotherm of supports (a) and catalysts (b).

**Table 2.** Textural data of samples.

Sample	BET Surface Area (m <sup>2</sup> /g)	Pore Volume (cm <sup>3</sup> /g)	Pore Diameter (nm)
Silicalite-1	454.31	0.32	2.85
TS-1-30	485.43	0.37	3.08
TS-1-20	471.39	0.37	3.16
Mn <sub>3</sub> Fe <sub>2</sub> /Silicalite-1	393.64	0.27	2.76
Mn <sub>3</sub> Fe <sub>2</sub> /TS-1-30	422.14	0.32	3.08
Mn <sub>3</sub> Fe <sub>2</sub> /TS-1-20	423.22	0.31	2.96

The morphologies of the catalysts are further investigated by SEM and transmission electron microscopy (TEM), with the results illustrated in Figure 4. The SEM images of catalysts present a typical MFI structure with a particle size of about 150 nm. However, the incorporation of Ti species results in some nanoscale folds on the surface of the catalysts, which can be attributed to the difference of atom size between Ti and Si. The active metal oxides are highly dispersed on the surface of catalysts in the form of small particles from the TEM images. As shown in Figure 5, the element mapping by energy-disperse X-ray spectroscopy (EDS) is applied to further identify the compositions of these small particles on the surface of the catalysts (EDS mappings of the supporters are shown in Figure S1). It can be found from Figure 5 that Mn, Fe and Ti species are all uniformly dispersed around the supporters. Besides, the results of Mn and Fe species are similar, indicating that Mn and Fe species may coexist in the form of FeMnO<sub>x</sub>, due to a strong interaction between metal oxides [33–35]. In summary, the introduction of Ti species does not change the textural properties of catalysts, but the surface of the catalysts is wrinkled, due to the difference of atom size between Ti and Si, which may provide better active sites for the catalytic reaction.

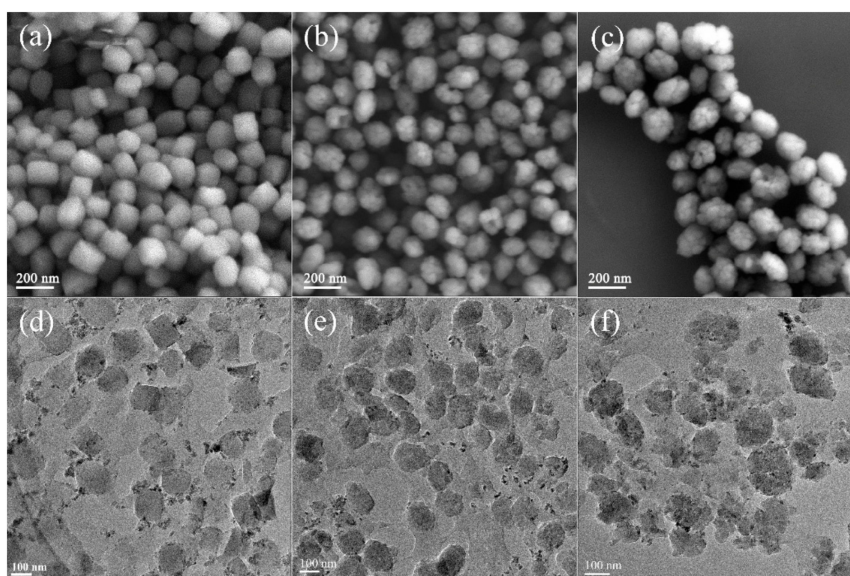


**Figure 4.** SEM and transmission electron microscopy (TEM) images of catalysts: (a,d) Mn<sub>3</sub>Fe<sub>2</sub>/Silicalite-1; (b,e) Mn<sub>3</sub>Fe<sub>2</sub>/TS-1-30; (c,f) Mn<sub>3</sub>Fe<sub>2</sub>/TS-1-20.

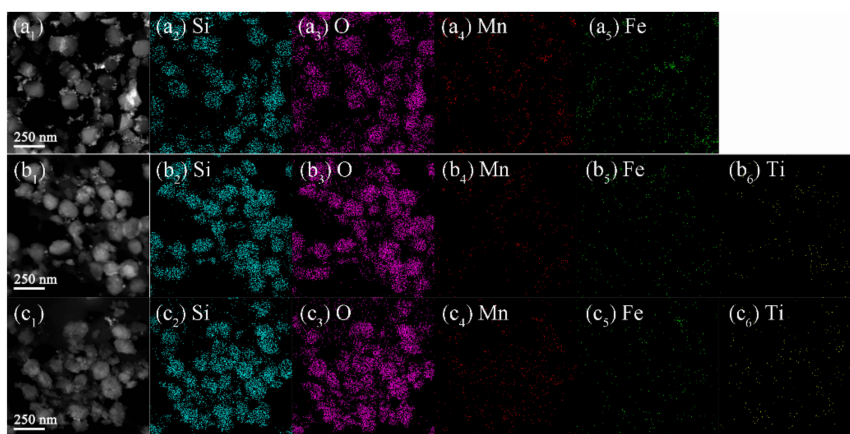


**Figure 5.** STEM images and energy-disperse X-ray spectroscopy (EDS) mappings of catalysts: (a)  $\text{Mn}_3\text{Fe}_2/\text{Silicalite-1}$ ; (b)  $\text{Mn}_3\text{Fe}_2/\text{TS-1-30}$ ; (c)  $\text{Mn}_3\text{Fe}_2/\text{TS-1-20}$ .

## 2.2. Surface Constituent and Chemical States of Samples

Figure 6 displays the XPS spectra of Mn 2p, Fe 2p and O 1s for different catalysts, and the results are summarized in Table 3. It can be seen from Figure 6a that the Mn 2p spectra consist of two major peaks that are assigned to Mn  $2p_{3/2}$  (peak around 642 eV) and  $2p_{1/2}$  (peak around 654 eV). The Mn  $2p_{3/2}$  peak can be fitted by three peaks (around 642 eV, 643 eV and 645 eV), which can be assigned to  $\text{Mn}^{2+}$ ,  $\text{Mn}^{3+}$  and  $\text{Mn}^{4+}$ , respectively [36,37]. Figure 6b displays the spectra of Fe 2p, which contains two main peaks relevant to Fe  $2p_{3/2}$  (peak around 710 eV) and  $2p_{1/2}$  (peak around 725 eV). The Fe  $2p_{3/2}$  can be separated into two independent peaks (around 713 eV, 710.7 eV), which can be assigned to  $\text{Fe}^{2+}$  and  $\text{Fe}^{3+}$  [13,38,39]. Regarding the oxygen species, O 1s spectra are shown in Figure 6c. The spectra can be separated into two peaks that related to the lattice oxygen (peak around 530 eV, labeled as  $\text{O}_\alpha$ ) and surface adsorbed oxygen (peak around 533 eV, labeled as  $\text{O}_\beta$ ) [40,41], respectively.

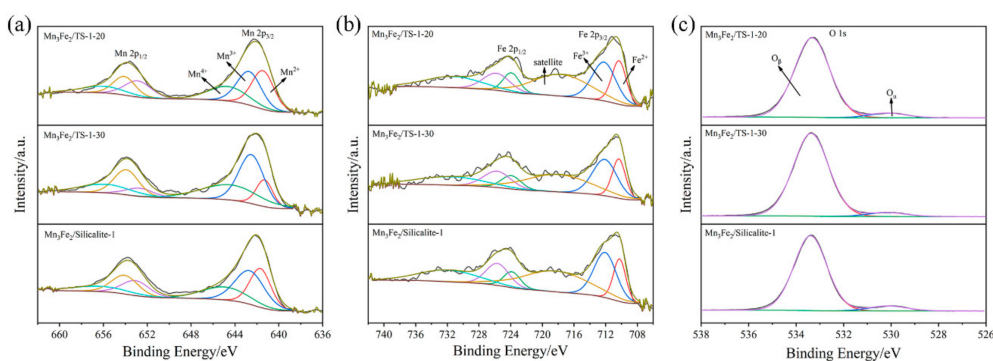


**Figure 6.** XPS spectra of catalysts: (a) Mn 2p; (b) Fe 2p; (c) O 1s.

**Table 3.** Surface atom concentrations of samples.

Sample	Atomic Concentration/at%				
	Si	O	Mn	Fe	Ti
$\text{Mn}_3\text{Fe}_2/\text{TS-1-20}$	37.37	61.78	0.53	0.13	0.19
$\text{Mn}_3\text{Fe}_2/\text{TS-1-30}$	37.33	61.86	0.50	0.15	0.16
$\text{Mn}_3\text{Fe}_2/\text{Silicalite-1}$	37.07	62.22	0.52	0.19	-

It is broadly reported that  $\text{Mn}^{4+}$  species play a major role in low-temperature  $\text{NH}_3$ -SCR reactions [37,42]. Hence, the ratios of  $\text{Mn}^{4+}/(\text{Mn}^{4+} + \text{Mn}^{3+} + \text{Mn}^{2+})$  over the catalysts are calculated and listed in Table 4, together with the ratios of  $\text{Fe}^{3+}/(\text{Fe}^{3+} + \text{Fe}^{2+})$  and  $\text{O}_\beta/(\text{O}_\alpha + \text{O}_\beta)$ , which are related to the catalytic performance of catalysts [30,43,44]. The  $\text{Mn}^{4+}/(\text{Mn}^{4+} + \text{Mn}^{3+} + \text{Mn}^{2+})$  ratio of

Mn<sub>3</sub>Fe<sub>2</sub>/TS-1-30 is 34.6%, which is a significant increase compared to that of Mn<sub>3</sub>Fe<sub>2</sub>/Silicalite-1 (25.0%). The increase of the Mn<sup>4+</sup> ratio can be attributed to the redox reactions between Mn and Ti species such as Mn<sup>3+</sup> + Ti<sup>4+</sup> = Mn<sup>4+</sup> + Ti<sup>3+</sup>, Mn<sup>2+</sup> + 2Ti<sup>4+</sup> = Mn<sup>4+</sup> + 2Ti<sup>3+</sup> [40]. However, the ratio of Mn<sup>4+</sup> remains unchanged in Mn<sub>3</sub>Fe<sub>2</sub>/TS-1-20, which can be attributed to the formation of anatase on the supporter. As mentioned above, the excessive Ti species generate anatase on the surface of the supporter, which is reported to inhibit the electron transfer between Mn species and the supporter [42]. The Fe<sup>3+</sup>/(Fe<sup>3+</sup> + Fe<sup>2+</sup>) ratio displays a slight decrease when the Ti species are introduced into the supporter, which can be attributed to redox equilibrium between Fe and Ti species like Fe<sup>3+</sup> + Ti<sup>3+</sup> = Fe<sup>2+</sup> + Ti<sup>4+</sup> [45]. According to the previously reported literature, surface adsorbed oxygen species (O<sub>β</sub>) show more reactive than lattice oxygen (O<sub>α</sub>) in the low-temperature NH<sub>3</sub>-SCR reaction, due to their outstanding mobility [46,47]. As shown in Table 4, the incorporation of Ti species increases the O<sub>β</sub>/(O<sub>α</sub> + O<sub>β</sub>) ratio, while the excessive Ti species consume the surface oxygen mainly because of the formation of anatase. In summary, Mn<sub>3</sub>Fe<sub>2</sub>/TS-1-30 tends to show the optimal catalytic performance, due to its highest ratio of Mn<sup>4+</sup> and surface adsorbed oxygen species.

**Table 4.** The chemical states and relative concentration ratios for different elements.

Samples	Atomic Ratio/%		
	Mn <sup>4+</sup> /(Mn <sup>4+</sup> + Mn <sup>3+</sup> + Mn <sup>2+</sup> )	Fe <sup>3+</sup> /(Fe <sup>3+</sup> + Fe <sup>2+</sup> )	O <sub>β</sub> /(O <sub>α</sub> + O <sub>β</sub> )
Mn <sub>3</sub> Fe <sub>2</sub> /TS-1-20	25.6	59.1	94.37
Mn <sub>3</sub> Fe <sub>2</sub> /TS-1-30	34.6	62.9	95.01
Mn <sub>3</sub> Fe <sub>2</sub> /Silicalite-1	25.0	65.5	93.01

### 2.3. Redox Properties of Samples

The redox properties of the catalysts are closely related to the catalytic performance in the NH<sub>3</sub>-SCR reaction. Therefore, H<sub>2</sub> temperature-programmed reduction (H<sub>2</sub>-TPR) is performed to characterize the redox properties of the catalysts and the results are exhibited in Figure 7 and Table 5. All the catalysts display three reduction peaks between 400 and 700 °C. The reduction peaks centered at 430 °C can be correlated with the simultaneous reduction of MnO<sub>2</sub> and Fe<sub>2</sub>O<sub>3</sub> (i.e., MnO<sub>2</sub> → Mn<sub>2</sub>O<sub>3</sub>, Mn<sub>2</sub>O<sub>3</sub> → Mn<sub>3</sub>O<sub>4</sub> and Fe<sub>2</sub>O<sub>3</sub> → FeO) [25,48]. The peaks centered at 580 °C can be assigned to the reduction of Mn<sub>3</sub>O<sub>4</sub>, while the peaks above 660 °C can be relevant to the reduction of FeO [48]. As shown in Table 5, when Ti species are introduced into the catalysts, the total area of the reduction peaks reaches 776 a.u., which has an increase of 20% compared to that in Mn<sub>3</sub>Fe<sub>2</sub>/Silicalite-1. Since the area of the reduction peak corresponds to the H<sub>2</sub> consumption, the redox properties of the catalysts are significantly enhanced after the incorporation of Ti species, which is beneficial to promote the NH<sub>3</sub>-SCR reaction at low temperatures.

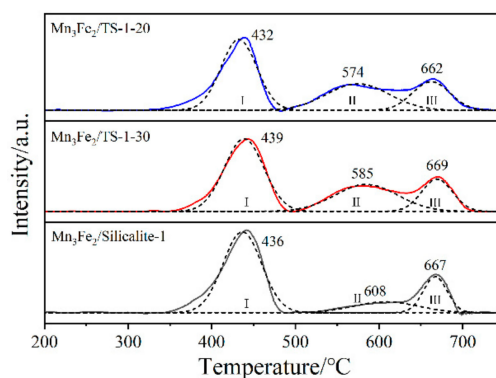


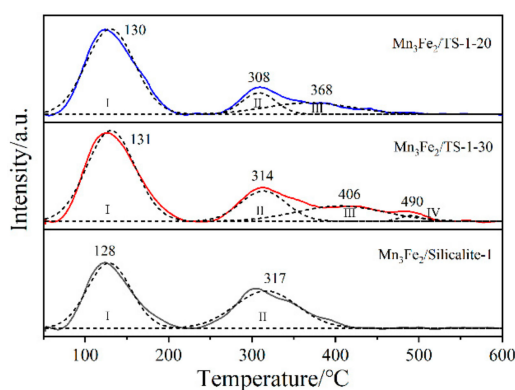
**Figure 7.** H<sub>2</sub> temperature-programmed reduction (H<sub>2</sub>-TPR) profiles of catalysts.

**Table 5.** The peak temperature and H<sub>2</sub> consumption of samples from H<sub>2</sub>-TPR.

Samples	Peak Temperature/°C			H <sub>2</sub> Consumption/a.u.			
	T <sub>I</sub>	T <sub>II</sub>	T <sub>III</sub>	S <sub>I</sub>	S <sub>II</sub>	S <sub>III</sub>	S <sub>total</sub>
Mn <sub>3</sub> Fe <sub>2</sub> /TS-1-20	432	574	662	356	231	150	737
Mn <sub>3</sub> Fe <sub>2</sub> /TS-1-30	439	585	669	400	236	140	776
Mn <sub>3</sub> Fe <sub>2</sub> /Silicalite-1	436	608	667	436	96	119	651

#### 2.4. Surface Acidity of Samples

The surface acidity is another important factor in low-temperature SCR reaction. Hence, NH<sub>3</sub> temperature-programmed desorption (NH<sub>3</sub>-TPD) is used to analyze the surface acidity of the catalysts, and the results are exhibited in Figure 8. For Mn<sub>3</sub>Fe<sub>2</sub>/Silicalite-1, it displays two desorption peaks labeled as I and II, which correspond to weak (<200 °C) and medium-strong (200~400 °C) acid sites, respectively [43,49]. However, more desorption peaks can be observed in Mn<sub>3</sub>Fe<sub>2</sub>/TS-1-30 and Mn<sub>3</sub>Fe<sub>2</sub>/TS-1-20, which are related to medium-strong acid sites [43,49], indicating that the new Lewis acid sites are related with the incorporation of Ti species and thus benefit the adsorption of NH<sub>3</sub>. The total acid amounts of these catalysts are calculated from TPD results and listed in Table 6. It shows that the acid amounts of Mn<sub>3</sub>Fe<sub>2</sub>/TS-1-30 and Mn<sub>3</sub>Fe<sub>2</sub>/TS-1-20 are larger than that of Mn<sub>3</sub>Fe<sub>2</sub>/Silicalite-1. Mn<sub>3</sub>Fe<sub>2</sub>/TS-1-30, especially, exhibits a remarkable increase (about 50%) in the acid amount, compared to that of Mn<sub>3</sub>Fe<sub>2</sub>/Silicalite-1. In summary, Ti species improve the surface acidity of the catalysts, which is beneficial for the adsorption of NH<sub>3</sub>, and finally enhances the catalytic performance in the low-temperature SCR reaction.

**Figure 8.** NH<sub>3</sub> temperature-programmed desorption (NH<sub>3</sub>-TPD) profiles of catalysts.**Table 6.** The peak temperature and acid amount of samples from NH<sub>3</sub>-TPD.

Samples	Peak Temperature/°C				Acid Amount/a.u.				
	T <sub>I</sub>	T <sub>II</sub>	T <sub>III</sub>	T <sub>IV</sub>	S <sub>I</sub>	S <sub>II</sub>	S <sub>III</sub>	S <sub>IV</sub>	S <sub>total</sub>
Mn <sub>3</sub> Fe <sub>2</sub> /TS-1-20	130	308	368	-	373	65	88	-	526
Mn <sub>3</sub> Fe <sub>2</sub> /TS-1-30	131	314	406	490	399	126	123	11	659
Mn <sub>3</sub> Fe <sub>2</sub> /Silicalite-1	128	317	-	-	259	213	-	-	472

Figure 9 displays the in situ diffuse reflectance infrared Fourier transform (in situ DRIFTS) of NH<sub>3</sub> adsorption in a temperature range between 60 and 330 °C, to further distinguish the Brønsted acid sites (labeled as B acid) and Lewis acid sites (labeled as L acid) on the surface of the catalysts. It is widely reported that the bands at 1602–1605 cm<sup>-1</sup>, 1225–1227 cm<sup>-1</sup>, 1142–1163 cm<sup>-1</sup> and 1059–1064 cm<sup>-1</sup> can be attributed to asymmetric and symmetric bending vibrations of the coordinated NH<sub>3</sub> linked to L acid sites [50,51]. The bands at 1428–1448 cm<sup>-1</sup> and 1737–1748 cm<sup>-1</sup> can be assigned to the NH<sub>4</sub><sup>+</sup> species on B acid sites [52]. The bands at 1550–1554 cm<sup>-1</sup> and 1302–1324 cm<sup>-1</sup> can be attributed to NH<sub>2</sub> species,

which are transformed from the coordinated  $\text{NH}_3$  [53,54]. Moreover, with the increase of temperature, the bands linked to B acid sites are found to decrease more noticeable than these linked to L acid sites, indicating that the bands assigned to L acid sites are more stable at a higher temperature [37]. Besides, by comparing the spectra of  $\text{Mn}_3\text{Fe}_2/\text{TS-1-30}$  (20) with that of  $\text{Mn}_3\text{Fe}_2/\text{Silicalite-1}$ , the intensity of bands at  $1602\text{--}1605\text{ cm}^{-1}$  and  $1428\text{--}1448\text{ cm}^{-1}$  is enhanced after the incorporation of Ti species, which indicates that  $\text{Mn}_3\text{Fe}_2/\text{TS-1-30}$  (20) can provide more adsorbed  $\text{NH}_3$  for SCR reaction than  $\text{Mn}_3\text{Fe}_2/\text{Silicalite-1}$ , which can benefit the catalytic activities.

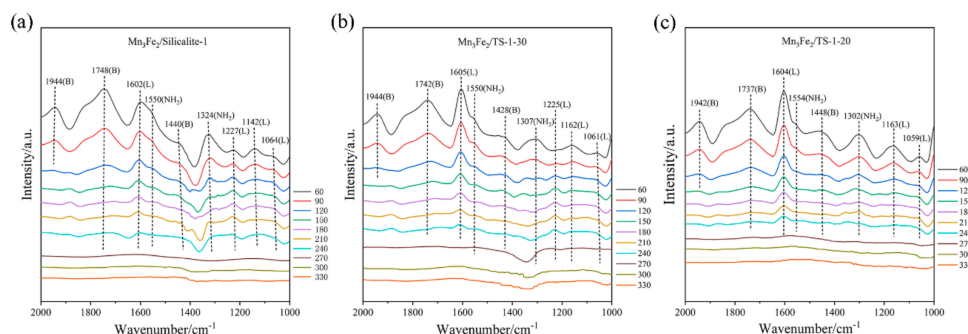


**Figure 9.** In situ diffuse reflectance infrared Fourier transform (in situ DRIFTS) of  $\text{NH}_3$  adsorption of depending on reaction temperatures from 60 to 330 °C: (a)  $\text{Mn}_3\text{Fe}_2/\text{Silicalite-1}$ ; (b)  $\text{Mn}_3\text{Fe}_2/\text{TS-1-30}$ ; (c)  $\text{Mn}_3\text{Fe}_2/\text{TS-1-20}$ .

### 2.5. Catalytic Performance of Samples

Figure 10a shows the catalytic activities of the catalysts under different reaction temperatures. It can be seen from the figure that  $\text{Mn}_3\text{Fe}_2/\text{TS-1-30}$  exhibits a  $\text{NO}_x$  conversion efficiency of 90% at 120 °C, which has an increase of almost 30% compared to that of  $\text{Mn}_3\text{Fe}_2/\text{Silicalite-1}$  at the same temperature. In addition, both  $\text{Mn}_3\text{Fe}_2/\text{TS-1-30}$  and  $\text{Mn}_3\text{Fe}_2/\text{TS-1-20}$  show an obvious improvement in catalytic activities at low temperatures, especially below 150 °C. The optimized catalysts,  $\text{Mn}_3\text{Fe}_2/\text{TS-1-30}$  can maintain steady  $\text{NO}_x$  conversion efficiencies above 80% in the temperature range between 110 and 230 °C, with a space velocity of  $18,000\text{ h}^{-1}$ . Based on the characterization of the catalysts' physical and chemical properties mentioned above, the improvement of low-temperature denitration activity is mainly attributed to the incorporation of Ti species, which enhances the redox properties of the catalysts and provides more surface acid sites for the adsorption of  $\text{NH}_3$ .

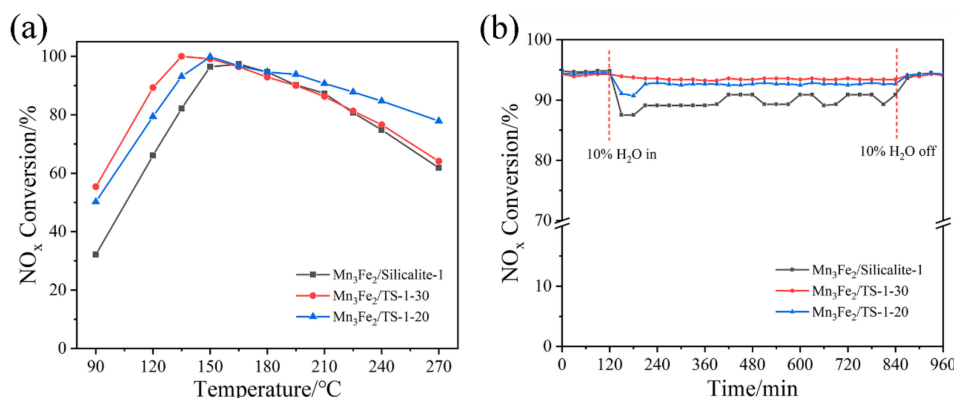


**Figure 10.** The  $\text{NH}_3$ -selective catalytic reduction (SCR) activity of catalysts at the variation of temperature (a);  $\text{H}_2\text{O}$  resistance performance of catalysts at 180 °C (b).

Since zeolites are reported to be sensitive to water vapor [26,28], the  $\text{H}_2\text{O}$  resistance of the catalysts is further studied at the temperature of 180 °C. As shown in Figure 10b, when 10 vol.%  $\text{H}_2\text{O}$  is introduced into the reaction,  $\text{Mn}_3\text{Fe}_2/\text{Silicalite-1}$  displays a decrease of about 5% in  $\text{NO}_x$  conversion

efficiency, while  $\text{Mn}_3\text{Fe}_2/\text{TS-1-30}$  remains unaffected by water vapor. It is widely accepted that the water deactivation is mainly because of the competitive adsorption between  $\text{NH}_3$  and water vapor [16,55], and the presence of Ti species further strengthens the hydrophobicity of the catalyst [29,56], thereby improving the  $\text{H}_2\text{O}$  resistance of the catalysts.

### 3. Materials and Methods

#### 3.1. Preparation of Samples

Silicalite-1 and TS-1 were synthesized by a hydrothermal template method, according to the previous literature [57,58]. The tetrapropylammonium hydroxide (TPAOH, 25 wt.% aqueous solution, Beijing Innochem Technology Co., Ltd., China) was served as a microporous template, while ethyl silicate (TEOS, Tianjin Guangfu Fine Chemical Research Institute, China) and tetrabutyl titanate (TBOT, Beijing Tongguang Fine Chemical Company, China) were served as the source of silicon and titanium, respectively. The molar composition of the synthesis solution was:  $\text{SiO}_2:\text{TiO}_2:\text{TPAOH}:\text{H}_2\text{O} = 1:(0\sim 0.05):0.2:7$ . Firstly, TEOS was added dropwise into 12.8 g aqueous solution of TPAOH at 40 °C with constant magnetic stirring while TBOT was dissolved in 10 g isopropanol. Secondly, the hydrolysis solutions of TEOS and TBOT were mixed and then heated up to 80 °C to distill off isopropanol. Then, the mixture was transferred into a stainless steel autoclave and then kept in an oven at 160 °C for 48 h. Afterwards, the white precipitation was washed by deionized water and ethanol for three times, respectively. Finally, the products were dried at 80 °C overnight, followed by calcination at 550 °C in the air for 6 h. The prepared samples without titanium labeled as Silicalite-1, while others with feeding  $n(\text{Si}/\text{Ti})$  of 30, 20 were labeled as TS-1-30 and TS-1-20, respectively.

$\text{MnO}_x\text{-FeO}_x$  catalysts were synthesized through the wet impregnation method. Manganese nitrate ( $\text{Mn}(\text{NO}_3)_2$ , 50 wt.% aqueous solution, Saen Chemical Technology (Shanghai) Co., Ltd., China) and iron nitrate nonahydrate ( $\text{Fe}(\text{NO}_3)_3\cdot 9\text{H}_2\text{O}$ , 99.9%, Beijing Tongguang Fine Chemical Company, China) were dissolved in deionized water as precursors and zeolites including Silicalite-1 and TS-1 were immersed into solution as supporters. The mass ratio of the mixture was:  $\text{Mn}:\text{Fe}:\text{supporter}$  (Silicalite-1 or TS-1) = 3:2:100, which is favorable for  $\text{NH}_3$ -SCR reaction according to the previous-reported researches [25,30]. After magnetic stirring at room temperature for 2 h, the mixture was transferred into an oven at 110 °C overnight, and followed by calcination at 500 °C in the air for 4 h. The samples were labeled as  $\text{Mn}_3\text{Fe}_2/\text{Silicalite-1}$ ,  $\text{Mn}_3\text{Fe}_2/\text{TS-1-30}$  and  $\text{Mn}_3\text{Fe}_2/\text{TS-1-20}$ , respectively.

#### 3.2. Characterization

X-ray diffraction (XRD) patterns of as-prepared samples were collected by a powder X-ray diffractometer (Rigaku Dmax-2400, RIGAKU, Tokyo, Japan) with  $\text{Cu-K}\alpha$  target. Fourier transform infrared (FT-IR) spectra were collected on a FT-IR spectrophotometer (Nicolet iS50, ThermoFisher, Waltham, MA, USA). The textural properties of as-prepared samples were investigated using a nitrogen adsorption apparatus (ASAP2020, Micromeritics, Norcross, GA, USA) at 77 K. Specific surface area, pore volume and pore size were calculated by Brunauer-Emmett-Teller (BET), single point and Barrett-Joyner-Halenda (BJH) methods, respectively. Surface morphologies of as-prepared samples were carried out on a field emission scanning electron microscope (Merlin Compact, ZEISS, Oberkochen, Germany) operating at 10 kV. Transmission electron microscopy (TEM) images of as-prepared samples were screened on a transmission electron microscope (JEM-2100F, JEOL, Tokyo, Japan) operating at 200 kV. The chemical composition of as-prepared samples was measured by an inductively coupled plasma-atomic emission spectrometer (Thermo iCAP6000 ICP-OES, ThermoFisher, Waltham, MA, USA). The surface chemical species of as-prepared samples were characterized by an X-ray photoelectron spectroscopy (AXIS Supra, Kratos Analytical Ltd., Manchester, UK) with  $\text{Al K}\alpha$  radiation.  $\text{H}_2$  temperature-programmed reduction ( $\text{H}_2$ -TPR) and  $\text{NH}_3$  temperature-programmed desorption ( $\text{NH}_3$ -TPD) experiments were carried out on a chemisorption analyzer (ChemBET Pulsar TPR/TPD, Quantachrome, Boynton Beach, FL, USA). In situ diffuse reflectance infrared Fourier

transform (in situ DRIFTS) of  $\text{NH}_3$  adsorption were obtained from a FT-IR spectrophotometer (Nicolet 6700, Thermo Fisher, USA), by accumulating 32 scans with a resolution of  $4 \text{ cm}^{-1}$ . The samples were firstly pretreated under a high purified  $\text{N}_2$  stream at  $400 \text{ }^\circ\text{C}$  for 1 h to remove physisorbed water and other impurities. Then the background spectra were obtained at target temperatures during the cooling procedure. Subsequently, the samples were exposed to a stream of  $\text{NH}_3/\text{N}_2$  (1 vol.%  $\text{NH}_3$ ) at room temperature, followed by purging with  $\text{N}_2$  for 30 min. The desorption of  $\text{NH}_3$  studies were measured by heating pre-adsorbed samples, and the spectra were recorded at stepped target temperatures by eliminating the corresponding background reference.

### 3.3. $\text{NH}_3$ -SCR Activity Measurements

The  $\text{NH}_3$ -SCR catalytic performances were tested in a fixed-bed quartz reactor (6 mm of internal diameter) in the temperature range from 90 to  $270 \text{ }^\circ\text{C}$ , with a GHSV of  $18,000 \text{ h}^{-1}$ . The reaction gas mixture was consisted of 500 ppm NO, 500 ppm  $\text{NH}_3$ , 3 vol.%  $\text{O}_2$ , 10 vol.%  $\text{H}_2\text{O}$  (if applied) and  $\text{N}_2$  in balance. Firstly, 200 mg catalyst was pretreated with  $\text{N}_2$  at  $200 \text{ }^\circ\text{C}$  for 30 min to eliminate physisorbed water. The concentrations of NO and  $\text{NO}_2$  were obtained through a flue gas analyzer (Testo 350 Pro, Testo, Black forest, Germany) when the catalytic reaction substantially reached a steady state at every target temperature. Moreover,  $\text{H}_2\text{O}$  resistance of the catalysts for low-temperature  $\text{NH}_3$ -SCR reaction was evaluated at the target temperature.  $\text{NO}_x$  conversion efficiency was calculated according to the following formula:

$$\text{NO}_x \text{ conversion efficiency}(\%) = \left(1 - \frac{[\text{NO}_x]_{\text{out}}}{[\text{NO}_x]_{\text{in}}}\right) \times 100\% \quad (1)$$

$$[\text{NO}_x] = [\text{NO}] + [\text{NO}_2] \quad (2)$$

where  $[\text{NO}_x]_{\text{in}}$  and  $[\text{NO}_x]_{\text{out}}$  refer to inlet and outlet concentrations of  $\text{NO}_x$  at steady state, respectively.

## 4. Conclusions

In this work, silicalite-1 and TS-1 were applied as supporters to load  $\text{MnO}_x$  and  $\text{FeO}_x$  nanoparticles as active components for the low-temperature  $\text{NH}_3$ -SCR reaction.  $\text{Mn}_3\text{Fe}_2/\text{TS-1-30}$  maintains  $\text{NO}_x$  conversion efficiencies above 80% when the range of temperature is from 110 to  $230 \text{ }^\circ\text{C}$ . Moreover,  $\text{Mn}_3\text{Fe}_2/\text{TS-1-30}$  can maintain a denitration efficiency of 94% in the presence of 10 vol.%  $\text{H}_2\text{O}$  at  $180 \text{ }^\circ\text{C}$  for over 12 h. Its excellent catalytic performance and  $\text{H}_2\text{O}$  resistance can be attributed to having much more surface acid sites and the stronger redox ability of its active components, which can be explained by the incorporation of Ti species. Therefore, the superior denitration ability and  $\text{H}_2\text{O}$  resistance of  $\text{Mn}_3\text{Fe}_2/\text{TS-1-30}$  will make it a practical catalyst for industrial largescale denitration at low temperatures.

**Supplementary Materials:** The following are available online at <http://www.mdpi.com/2073-4344/10/5/566/s1>, Figure S1: STEM images and EDS mappings of the supporters: (a) TS-1-30; (b) TS-1-20.

**Author Contributions:** Conceptualization, J.G. and X.W.; formal analysis, J.G., R.D. and Y.C.; writing—original draft preparation, J.G.; writing—review and editing, J.G., R.D., W.C. and X.W.; supervision, X.W.; project administration, L.L.; funding acquisition, L.L. and X.W. All authors have read and agreed to the published version of the manuscript.

**Funding:** This research was funded by the National Natural Science Foundation of China (Grant No. 51672006 and 51472006), the Ministry of Land and Resources Public Welfare Industry Research Project (No. 201511062-02) and the National key research and development plan (No. 2018YFC1901505).

**Conflicts of Interest:** The authors declare no conflict of interest.

## References

1. Busca, G.; Lietti, L.; Ramis, G.; Berti, F. Chemical and mechanistic aspects of the selective catalytic reduction of NO<sub>x</sub> by ammonia over oxide catalysts: A review. *Appl. Catal. B Environ.* **1998**, *18*, 1–36. [[CrossRef](#)]
2. Wang, X.; Liu, Y.; Wu, Z. Highly active NbOPO<sub>4</sub> supported Cu-Ce catalyst for NH<sub>3</sub>-SCR reaction with superior sulfur resistance. *Chem. Eng. J.* **2020**, *382*, 122941. [[CrossRef](#)]
3. Paolucci, C.; Khurana, I.; Parekh, A.A.; Li, S.; Shih, A.J.; Li, H.; Di Iorio, J.R.; Albarracin-Caballero, J.D.; Yezerets, A.; Miller, J.T.; et al. Dynamic multinuclear sites formed by mobilized copper ions in NO<sub>x</sub> selective catalytic reduction. *Science* **2017**, *357*, 898–903. [[CrossRef](#)]
4. Gillot, S.; Tricot, G.; Vezin, H.; Dacquin, J.-P.; Dujardin, C.; Granger, P. Development of stable and efficient CeVO<sub>4</sub> systems for the selective reduction of NO<sub>x</sub> by ammonia: Structure-activity relationship. *Appl. Catal. B Environ.* **2017**, *218*, 338–348. [[CrossRef](#)]
5. Mou, X.; Zhang, B.; Li, Y.; Yao, L.; Wei, X.; Su, D.S.; Shen, W. Rod-Shaped Fe<sub>2</sub>O<sub>3</sub> as an Efficient Catalyst for the Selective Reduction of Nitrogen Oxide by Ammonia. *Angew. Chem. Int. Ed.* **2012**, *51*, 2989. [[CrossRef](#)]
6. Chen, L.; Si, Z.; Wu, X.; Weng, D. DRIFT study of CuO-CeO<sub>2</sub>-TiO<sub>2</sub> mixed oxides for NO<sub>x</sub> reduction with NH<sub>3</sub> at low temperatures. *ACS Appl. Mater. Interfaces* **2014**, *6*, 8134–8145. [[CrossRef](#)]
7. Gao, F.; Tang, X.; Yi, H.; Li, J.; Zhao, S.; Wang, J.; Chu, C.; Li, C. Promotional mechanisms of activity and SO<sub>2</sub> tolerance of Co- or Ni-doped MnO<sub>x</sub>-CeO<sub>2</sub> catalysts for SCR of NO<sub>x</sub> with NH<sub>3</sub> at low temperature. *Chem. Eng. J.* **2017**, *317*, 20–31. [[CrossRef](#)]
8. Fang, C.; Zhang, D.; Cai, S.; Zhang, L.; Huang, L.; Li, H.; Maitarad, P.; Shi, L.; Gao, R.; Zhang, J. Low-temperature selective catalytic reduction of NO with NH<sub>3</sub> over nanoflaky MnO<sub>x</sub> on carbon nanotubes in situ prepared via a chemical bath deposition route. *Nanoscale* **2013**, *5*, 9199. [[CrossRef](#)] [[PubMed](#)]
9. Chen, Y.; Zhang, Z.; Liu, L.; Mi, L.; Wang, X. In situ DRIFTS studies on MnO<sub>x</sub> nanowires supported by activated semi-coke for low temperature selective catalytic reduction of NO<sub>x</sub> with NH<sub>3</sub>. *Appl. Surf. Sci.* **2016**, *366*, 139–147. [[CrossRef](#)]
10. Zhang, C.; Chen, T.; Liu, H.; Chen, D.; Xu, B.; Qing, C. Low temperature SCR reaction over Nano-Structured Fe-Mn Oxides: Characterization, performance, and kinetic study. *Appl. Surf. Sci.* **2018**, *457*, 1116–1125. [[CrossRef](#)]
11. Yang, J.; Ren, S.; Zhang, T.; Su, Z.; Long, H.; Kong, M.; Yao, L. Iron doped effects on active sites formation over activated carbon supported Mn-Ce oxide catalysts for low-temperature SCR of NO. *Chem. Eng. J.* **2020**, *379*, 122398. [[CrossRef](#)]
12. Pan, W.-G.; Hong, J.-N.; Guo, R.-T.; Zhen, W.-L.; Ding, H.-L.; Jin, Q.; Ding, C.-G.; Guo, S.-Y. Effect of support on the performance of Mn-Cu oxides for low temperature selective catalytic reduction of NO with NH<sub>3</sub>. *J. Ind. Eng. Chem.* **2014**, *20*, 2224–2227. [[CrossRef](#)]
13. Chen, Z.; Wang, F.; Li, H.; Yang, Q.; Wang, L.; Li, X. Low-Temperature Selective Catalytic Reduction of NO<sub>x</sub> with NH<sub>3</sub> over Fe-Mn Mixed-Oxide Catalysts Containing Fe<sub>3</sub>Mn<sub>3</sub>O<sub>8</sub> Phase. *Ind. Eng. Chem. Res.* **2011**, *51*, 202–212. [[CrossRef](#)]
14. Liu, Z.; Yi, Y.; Zhang, S.; Zhu, T.; Zhu, J.; Wang, J. Selective catalytic reduction of NO<sub>x</sub> with NH<sub>3</sub> over Mn-Ce mixed oxide catalyst at low temperatures. *Catal. Today* **2013**, *216*, 76–81. [[CrossRef](#)]
15. Li, J.H.; Chang, H.Z.; Ma, L.; Hao, J.M.; Yang, R.T. Low-temperature selective catalytic reduction of NO<sub>x</sub> with NH<sub>3</sub> over metal oxide and zeolite catalysts-A review. *Catal. Today* **2011**, *175*, 147–156. [[CrossRef](#)]
16. Liu, C.; Shi, J.-W.; Gao, C.; Niu, C. Manganese oxide-based catalysts for low-temperature selective catalytic reduction of NO<sub>x</sub> with NH<sub>3</sub>: A review. *Appl. Catal. A Gen.* **2016**, *522*, 54–69. [[CrossRef](#)]
17. Wu, S.; Zhang, L.; Wang, X.; Zou, W.; Cao, Y.; Sun, J.; Tang, C.; Gao, F.; Deng, Y.; Dong, L. Synthesis, characterization and catalytic performance of FeMnTiO<sub>x</sub> mixed oxides catalyst prepared by a CTAB-assisted process for mid-low temperature NH<sub>3</sub>-SCR. *Appl. Catal. A Gen.* **2015**, *505*, 235–242. [[CrossRef](#)]
18. Cao, F.; Su, S.; Xiang, J.; Wang, P.; Hu, S.; Sun, L.; Zhang, A. The activity and mechanism study of Fe-Mn-Ce/γ-Al<sub>2</sub>O<sub>3</sub> catalyst for low temperature selective catalytic reduction of NO with NH<sub>3</sub>. *Fuel* **2015**, *139*, 232–239. [[CrossRef](#)]
19. Chen, Y.; Wang, J.; Yan, Z.; Liu, L.; Zhang, Z.; Wang, X. Promoting effect of Nd on the reduction of NO with NH<sub>3</sub> over CeO<sub>2</sub> supported by activated semi-coke: An in situ DRIFTS study. *Catal. Sci. Technol.* **2015**, *5*, 2251–2259. [[CrossRef](#)]

20. Wang, J.; Yan, Z.; Liu, L.; Chen, Y.; Zhang, Z.; Wang, X. In situ DRIFTS investigation on the SCR of NO with NH<sub>3</sub> over V<sub>2</sub>O<sub>5</sub> catalyst supported by activated semi-coke. *Appl. Surf. Sci.* **2014**, *313*, 660–669. [[CrossRef](#)]
21. Su, Y.; Fan, B.; Wang, L.; Liu, Y.; Huang, B.; Fu, M.; Chen, L.; Ye, D. MnO<sub>x</sub> supported on carbon nanotubes by different methods for the SCR of NO with NH<sub>3</sub>. *Catal. Today* **2013**, *201*, 115–121. [[CrossRef](#)]
22. Lou, X.; Liu, P.; Li, J.; Li, Z.; He, K. Effects of calcination temperature on Mn species and catalytic activities of Mn/ZSM-5 catalyst for selective catalytic reduction of NO with ammonia. *Appl. Surf. Sci.* **2014**, *307*, 382–387. [[CrossRef](#)]
23. Seo, C.-K.; Choi, B.; Kim, H.; Lee, C.-H.; Lee, C.-B. Effect of ZrO<sub>2</sub> addition on de-NO<sub>x</sub> performance of Cu-ZSM-5 for SCR catalyst. *Chem. Eng. J.* **2012**, *191*, 331–340. [[CrossRef](#)]
24. Lv, G.; Bin, F.; Song, C.; Wang, K.; Song, J. Promoting effect of zirconium doping on Mn/ZSM-5 for the selective catalytic reduction of NO with NH<sub>3</sub>. *Fuel* **2013**, *107*, 217–224. [[CrossRef](#)]
25. Wang, T.; Wan, Z.; Yang, X.; Zhang, X.; Niu, X.; Sun, B. Promotional effect of iron modification on the catalytic properties of Mn-Fe/ZSM-5 catalysts in the Fast SCR reaction. *Fuel Process. Technol.* **2018**, *169*, 112–121. [[CrossRef](#)]
26. Du, T.; Qu, H.; Liu, Q.; Zhong, Q.; Ma, W. Synthesis, activity and hydrophobicity of Fe-ZSM-5@silicalite-1 for NH<sub>3</sub>-SCR. *Chem. Eng. J.* **2015**, *262*, 1199–1207. [[CrossRef](#)]
27. Vu, D.V.; Miyamoto, M.; Nishiyama, N.; Ichikawa, S.; Egashira, Y.; Ueyama, K. Catalytic activities and structures of silicalite-1/H-ZSM-5 zeolite composites. *Microporous Mesoporous Mater.* **2008**, *115*, 106–112. [[CrossRef](#)]
28. Serrano, D.P.; Calleja, G.; Botas, J.A.; Gutierrez, F.J. Characterization of adsorptive and hydrophobic properties of silicalite-1, ZSM-5, TS-1 and Beta zeolites by TPD techniques. *Sep. Purif. Technol.* **2007**, *54*, 1–9. [[CrossRef](#)]
29. Li, G.; Wang, X.; Guo, X.; Liu, S.; Zhao, Q.; Bao, X.; Lin, L. Titanium species in titanium silicalite TS-1 prepared by hydrothermal method. *Mater. Chem. Phys.* **2001**, *71*, 195–201. [[CrossRef](#)]
30. Mu, W.; Zhu, J.; Zhang, S.; Guo, Y.; Su, L.; Li, X.; Li, Z. Novel proposition on mechanism aspects over Fe-Mn/ZSM-5 catalyst for NH<sub>3</sub>-SCR of NO<sub>x</sub> at low temperature: Rate and direction of multifunctional electron-transfer-bridge and in situ DRIFTS analysis. *Catal. Sci. Technol.* **2016**, *6*, 7532–7548. [[CrossRef](#)]
31. Xia, Y.; Zhan, W.; Guo, Y.; Guo, Y.; Lu, G. Fe-Beta zeolite for selective catalytic reduction of NO<sub>x</sub> with NH<sub>3</sub>: Influence of Fe content. *Chin. J. Catal.* **2016**, *37*, 2069–2078. [[CrossRef](#)]
32. Xu, W.; Zhang, G.; Chen, H.; Zhang, G.; Han, Y.; Chang, Y.; Gong, P. Mn/beta and Mn/ZSM-5 for the low-temperature selective catalytic reduction of NO with ammonia: Effect of manganese precursors. *Chin. J. Catal.* **2018**, *39*, 118–127. [[CrossRef](#)]
33. Cheng, K.; Liu, J.; Zhao, Z.; Wei, Y.; Jiang, G.; Duan, A. Direct synthesis of V-W-Ti nanoparticle catalysts for selective catalytic reduction of NO with NH<sub>3</sub>. *RSC Adv.* **2015**, *5*, 45172–45183. [[CrossRef](#)]
34. Hu, H.; Cai, S.; Li, H.; Huang, L.; Shi, L.; Zhang, D. In Situ DRIFTS Investigation of the Low-Temperature Reaction Mechanism over Mn-Doped Co<sub>3</sub>O<sub>4</sub> for the Selective Catalytic Reduction of NO<sub>x</sub> with NH<sub>3</sub>. *J. Phys. Chem. C* **2015**, *119*, 22924–22933. [[CrossRef](#)]
35. Liu, F.; He, H.; Ding, Y.; Zhang, C. Effect of manganese substitution on the structure and activity of iron titanate catalyst for the selective catalytic reduction of NO with NH<sub>3</sub>. *Appl. Catal. B Environ.* **2009**, *93*, 194–204. [[CrossRef](#)]
36. Reddy, A.; Gopinath, C.; Chilukuri, S. Selective ortho-methylation of phenol with methanol over copper manganese mixed-oxide spinel catalysts. *J. Catal.* **2006**, *243*, 278–291. [[CrossRef](#)]
37. Xiong, Y.; Tang, C.; Yao, X.; Zhang, L.; Li, L.; Wang, X.; Deng, Y.; Gao, B.; Dong, L. Effect of metal ions doping (M=Ti<sup>4+</sup>, Sn<sup>4+</sup>) on the catalytic performance of MnO<sub>x</sub>/CeO<sub>2</sub> catalyst for low temperature selective catalytic reduction of NO with NH<sub>3</sub>. *Appl. Catal. A Gen.* **2015**, *495*, 206–216. [[CrossRef](#)]
38. Zhu, L.; Zhang, L.; Qu, H.; Zhong, Q. A study on chemisorbed oxygen and reaction process of Fe-CuO<sub>x</sub>/ZSM-5 via ultrasonic impregnation method for low-temperature NH<sub>3</sub>-SCR. *J. Mol. Catal. A Chem.* **2015**, *409*, 207–215. [[CrossRef](#)]
39. Tan, P. Active phase, catalytic activity, and induction period of Fe/zeolite material in nonoxidative aromatization of methane. *J. Catal.* **2016**, *338*, 21–29. [[CrossRef](#)]
40. Li, L.; Wu, Y.; Hou, X.; Chu, B.; Nan, B.; Qin, Q.; Fan, M.; Sun, C.; Li, B.; Dong, L.; et al. Investigation of Two-Phase Intergrowth and Coexistence in Mn-Ce-Ti-O Catalysts for the Selective Catalytic Reduction of NO with NH<sub>3</sub>: Structure-Activity Relationship and Reaction Mechanism. *Ind. Eng. Chem. Res.* **2018**, *58*, 849–862. [[CrossRef](#)]

41. Meng, D.; Zhan, W.; Guo, Y.; Guo, Y.; Wang, L.; Lu, G. A Highly Effective Catalyst of Sm-MnO<sub>x</sub> for the NH<sub>3</sub>-SCR of NO<sub>x</sub> at Low Temperature: Promotional Role of Sm and Its Catalytic Performance. *ACS Catal.* **2015**, *5*, 5973–5983. [[CrossRef](#)]
42. Yao, X.; Chen, L.; Cao, J.; Chen, Y.; Tian, M.; Yang, F.; Sun, J.; Tang, C.; Dong, L. Enhancing the deNO performance of MnO<sub>x</sub>/CeO<sub>2</sub>-ZrO<sub>2</sub> nanorod catalyst for low-temperature NH<sub>3</sub>-SCR by TiO<sub>2</sub> modification. *Chem. Eng. J.* **2019**, *369*, 46–56. [[CrossRef](#)]
43. You, X.; Sheng, Z.; Yu, D.; Yang, L.; Xiao, X.; Wang, S. Influence of Mn/Ce ratio on the physicochemical properties and catalytic performance of graphene supported MnO<sub>x</sub>-CeO<sub>2</sub> oxides for NH<sub>3</sub>-SCR at low temperature. *Appl. Surf. Sci.* **2017**, *423*, 845–854. [[CrossRef](#)]
44. Zha, K.; Cai, S.; Hu, H.; Li, H.; Yan, T.; Shi, L.; Zhang, D. In Situ DRIFTS Investigation of Promotional Effects of Tungsten on MnO<sub>x</sub>-CeO<sub>2</sub>/meso-TiO<sub>2</sub> Catalysts for NO<sub>x</sub> Reduction. *J. Phys. Chem. C* **2017**, *121*, 25243–25254. [[CrossRef](#)]
45. Kang, M.; Park, E.D.; Kim, J.M.; Yie, J.E. Cu–Mn mixed oxides for low temperature NO reduction with NH<sub>3</sub>. *Catal. Today* **2006**, *111*, 236–241. [[CrossRef](#)]
46. Chen, J.; Chen, X.; Chen, X.; Xu, W.; Xu, Z.; Jia, H.; Chen, J. Homogeneous introduction of CeO<sub>y</sub> into MnO<sub>x</sub>-based catalyst for oxidation of aromatic VOCs. *Appl. Catal. B Environ.* **2018**, *224*, 825–835. [[CrossRef](#)]
47. Du, J.; Qu, Z.; Dong, C.; Song, L.; Qin, Y.; Huang, N. Low-temperature abatement of toluene over Mn–Ce oxides catalysts synthesized by a modified hydrothermal approach. *Appl. Surf. Sci.* **2018**, *433*, 1025–1035. [[CrossRef](#)]
48. Lin, L.-Y.; Lee, C.-Y.; Zhang, Y.-R.; Bai, H. Aerosol-assisted deposition of Mn-Fe oxide catalyst on TiO<sub>2</sub> for superior selective catalytic reduction of NO with NH<sub>3</sub> at low temperatures. *Catal. Commun.* **2018**, *111*, 36–41. [[CrossRef](#)]
49. Peng, Y.; Wang, D.; Li, B.; Wang, C.; Li, J.; Crittenden, J.; Hao, J. Impacts of Pb and SO<sub>2</sub> Poisoning on CeO<sub>2</sub>-WO<sub>3</sub>/TiO<sub>2</sub>-SiO<sub>2</sub> SCR Catalyst. *Environ. Sci. Technol.* **2017**, *51*, 11943–11949. [[CrossRef](#)]
50. Liu, Y.; Gu, T.; Weng, X.; Wang, Y.; Wu, Z.; Wang, H. DRIFT Studies on the Selectivity Promotion Mechanism of Ca-Modified Ce-Mn/TiO<sub>2</sub> Catalysts for Low-Temperature NO Reduction with NH<sub>3</sub>. *J. Phys. Chem. C* **2012**, *116*, 16582–16592. [[CrossRef](#)]
51. Ramis, G.; Yi, L.; Busca, G. Ammonia activation over catalysts for the selective catalytic reduction of NO<sub>x</sub> and the selective catalytic oxidation of NH<sub>3</sub>. An FT-IR study. *Catal. Today* **1996**, *28*, 373–380. [[CrossRef](#)]
52. Lin, S.D.; Gluhoi, A.C.; Nieuwenhuys, B.E. Ammonia oxidation over Au/MO/γ-Al<sub>2</sub>O<sub>3</sub>—activity, selectivity and FTIR measurements. *Catal. Today* **2004**, *90*, 3–14. [[CrossRef](#)]
53. Ettireddy, P.R.; Ettireddy, N.; Boningari, T.; Pardemann, R.; Smirniotis, P.G. Investigation of the selective catalytic reduction of nitric oxide with ammonia over Mn/TiO<sub>2</sub> catalysts through transient isotopic labeling and in situ FT-IR studies. *J. Catal.* **2012**, *292*, 53–63. [[CrossRef](#)]
54. Liu, Z.; Zhu, J.; Li, J.; Ma, L.; Woo, S.I. Novel Mn-Ce-Ti mixed-oxide catalyst for the selective catalytic reduction of NO<sub>x</sub> with NH<sub>3</sub>. *ACS Appl. Mater. Interfaces* **2014**, *6*, 14500–14508. [[CrossRef](#)] [[PubMed](#)]
55. Zhang, S.; Zhang, B.; Liu, B.; Sun, S. A review of Mn-containing oxide catalysts for low temperature selective catalytic reduction of NO<sub>x</sub> with NH<sub>3</sub>: Reaction mechanism and catalyst deactivation. *RSC Adv.* **2017**, *7*, 26226–26242. [[CrossRef](#)]
56. Chen, H.; Zhang, R.; Bao, W.; Wang, H.; Wang, Z.; Wei, Y. Effective catalytic abatement of indoor formaldehyde at room temperature over TS-1 supported platinum with relatively low content. *Catal. Today* **2019**. [[CrossRef](#)]
57. Kuperman, A.; Nadimi, S.; Oliver, S.; Ozin, G.A.; Garces, J.M.; Olken, M.M. Non-aqueous Synthesis of Giant Crystal of Zeolites and Molecular Sieves. *Nature* **1993**, *365*, 239–242. [[CrossRef](#)]
58. Zuo, Y.; Liu, M.; Zhang, T.; Hong, L.; Guo, X.; Song, C.; Chen, Y.; Zhu, P.; Jaye, C.; Fischer, D. Role of pentahedrally coordinated titanium in titanium silicalite-1 in propene epoxidation. *RSC Adv.* **2015**, *5*, 17897–17904. [[CrossRef](#)]

